



CHORUS

This is the accepted manuscript made available via CHORUS. The article has been published as:

Statistical inference approach to structural reconstruction of complex networks from binary time series

Chuang Ma, Han-Shuang Chen, Ying-Cheng Lai, and Hai-Feng Zhang

Phys. Rev. E **97**, 022301 — Published 5 February 2018

DOI: [10.1103/PhysRevE.97.022301](https://doi.org/10.1103/PhysRevE.97.022301)

A statistical inference approach to structural reconstruction of complex networks from binary time series

Chuang Ma,¹ Han-Shuang Chen,² Ying-Cheng Lai,³ and Hai-Feng Zhang^{1,4,5,*}

¹*School of Mathematical Science, Anhui University, Hefei 230601, China*

²*School of Physics and Material Science, Anhui University, Hefei 230601, China*

³*School of Electrical, Computer and Energy Engineering,*

Arizona State University, Tempe, Arizona 85287, USA

⁴*Center of Information Support & Assurance Technology, Anhui University, Hefei 230601, China*

⁵*Department of Communication Engineering, North University of China, Taiyuan, Shan'xi 030051, China*

(Dated: January 24, 2018)

Complex networks hosting binary-state dynamics arise in a variety of contexts. In spite of previous works, to fully reconstruct the network structure from observed binary data remains to be challenging. We articulate a statistical inference based approach to this problem. In particular, exploiting the expectation-maximization (EM) algorithm, we develop a method to ascertain the neighbors of any node in the network based solely on binary data, thereby recovering the full topology of the network. A key ingredient of our method is the maximum likelihood estimation of the probabilities associated with actual or non-existent links, and we show that the EM algorithm can distinguish the two kinds of probability values without any ambiguity, insofar as the length of the available binary time series is reasonably long. Our method does not require any *a priori* knowledge of the detailed dynamical processes, is parameter free, and is capable of accurate reconstruction even in the presence of noise. We demonstrate the method using combinations of distinct types of binary dynamical processes and network topologies, and provide a physical understanding of the underlying reconstruction mechanism. Our statistical inference based reconstruction method contributes an additional piece to the rapidly expanding “toolbox” of data based reverse engineering of complex networked systems.

I. INTRODUCTION

Data based reconstruction of complex networked systems has been an active area of research in network science and engineering with applications in a wide range of disciplines [1–43]. A tacit assumption in most existing works is that continuous-valued nodal time series, either in continuous or discrete time, are available so that various statistical measures can be computed for identifying the underlying network structure. This has led to a diverse array of reconstruction methodologies [1–44]. For example, from time series the traditional Pearson correlation can be calculated to reveal the complex structure of the brain functional and neural networks [6, 7, 45, 46]. Bayesian estimation has also been used for reconstructing neural networks [47, 48]. Based on continuous time series and knowledge about the nodal dynamical equations, a delayed feedback control scheme can be designed to reveal the network structure based on the principle of synchronization [8, 23]. For stochastic and nonlinear network dynamics that generate noisy, continuous time series, situations can arise where the network matrix is directly proportional to the dynamical correlation matrix that can be calculated straightforwardly from the time series, leading to a class of computationally efficient reconstruction methods [15, 17, 29, 36, 41]. When the data amount is small, i.e., when only short (continuous

or discrete) time series are available, the principle of compressive sensing [49] can be exploited to develop frameworks for a variety of reconstruction tasks [24–26, 38–40, 42, 43, 50]. (See Ref. [51] for a recent review.) We note that, in most previous works, the values of the measured time series are continuous in a range, regardless of whether time is continuous or discrete.

In real systems, there are network dynamical processes that generate binary time series, i.e., the values of the time series assume only two possible values, e.g., 0 or 1. For example, in disease spreading on a social network, the state of each node (person) can be conveniently characterized as susceptible or infected [52], which equally applies to virus propagation on computer networks. In certain class of neural networks, each node (neuron) can be classified as active or inactive [53]. In classical evolutionary game dynamics such as the prisoner dilemma game, each node can be in one of the two states: cooperation or defection [54, 55]. In a political network, the state of each node (the opinion of each individual) can be either “for” or “against” [56]. Because of the binary (or more generally, polarized) nature of the available data, the corresponding network reconstruction problem is difficult. In spite of the challenge, there have been previous efforts. For example, a compressive sensing based method was developed to reconstruct the propagation or diffusion network of disease spreading and to identify the source [40]. In this case, the network dynamical process is assumed to be known, e.g., the classical susceptible-infection-refractory (SIR) dynamics. For a variety of binary-state dynamics, a Boltzmann machine based on

* haifengzhang1978@gmail.com

the classical Ising model can be reconstructed from the polarized data to yield the network structure and nodal dynamics [57], but the computational demand is high, making the method effective but only for relatively small networks. Quite recently, a linearization approach was proposed [43] to approximate the nodal dynamical equations that generate the binary time series so as to convert network reconstruction into a sparse signal optimization problem, which can then be solved by the conventional lasso (least absolute shrinkage and selection operator) method from statistics and machine learning. The core of this linearization approach is to estimate the switching probabilities for a node to change from one state to another based on properly selected and averaged strings of binary time series, a process that requires fine adjustments of a number of algorithmic parameters to ensure that the selected strings are neither too special nor too similar to each other.

In this paper, we develop a statistical inference based method to reconstruct complex network structure from binary time series. The principle of statistical inference has recently been used in network science for tasks such as identifying the community structures for single-layer [58], multilayer [59], or signed [60] networks, and detecting the core-periphery structure for complex networks [61]. In general, the statistical inference method has a solid mathematical support and often can lead to robust performance. The key to structural reconstruction is to calculate the probability for an arbitrary pair of nodes to have a link. More importantly, it is necessary to distinguish the probability values associated with actual links and those with non-existent links. Accurate reconstruction demands that the two kinds of probability values be unequivocally distinguishable. Exploiting the expectation-maximization (EM) algorithm in statistical inference, we derive formulas for the probabilities with the finding of a generic feature: in all cases investigated there exists a finite gap between the two types of probability values. Surprisingly, the appealing gap feature is robust as it holds for a large number of combinations of the binary state dynamics with model and real complex network structures, and it continues to exist even when there are stochastic perturbations to the binary time series. As a result, a threshold probability value can be readily determined (and we provide a formula for it) to ascertain whether there is an actual link between any pair of nodes. The final outcome is an unprecedented high accuracy of network structural reconstruction. Another appealing feature of our reconstruction methodology is that no parameters are *a priori* assumed - all parameters can be estimated based on the available binary data. Our reconstruction method adds a piece into the rapidly expanding “toolbox” of reverse engineering of complex dynamical networks, a problem with broad applications.

II. STATISTICAL INFERENCE BASED MATHEMATICAL FORMULATION OF RECONSTRUCTION

For a networked system having binary-state dynamics, at any time a node can be in one of the two states: 0 (inactive) or 1 (active). The basic setting under which our method is applicable is that, for the underlying dynamical process, the probability of each node being activated at next time step is determined *only* by its active neighbors at the current step, so only transitions from inactive to active nodes are considered for the network reconstruction. The binary dynamical process is Markovian. Except for this condition, further details of the dynamical process are assumed to be unknown but only the binary time series of the nodal states are available.

In general, if the neighbors of each node can be accurately identified, the full topology and structure of the network can be ascertained. Consider a network of size N and M time steps during the dynamical evolution. The available data can be represented as an $M \times N$ matrix (labeled as S). For example, for the illustrative network structure in Fig. 1(a), the matrix representation of the data is the one shown in Fig. 1(b). Let $s_i(t)$ be the state of node i at time t , where $s_i(t) = 1$ if i is active [corresponding to the black squares in Fig. 1(b)] and $s_i(t) = 0$ if i is inactive [illustrated by the blank squares in Fig. 1(b)].

Let $i \rightarrow j$ denote the event that node i has a direct effect on the state of node j . For example, node i can spread a disease or send a piece of information to node j at time t . For the type of binary dynamical processes considered, we assume that the probability for each node to be activated is affected *only* by its active neighbors. As a result, node i has a direct effect on node j only when node i is one of the neighbors of node j . That is, the event $i \rightarrow j$ indicates whether node i is connected to node j , which is a property independent of time t . The conditional probability of $s_j(t+1) = 1$ and $i \rightarrow j$, given $s_i(t) = 1$ and $s_j(t) = 0$, is

$$\begin{aligned} P_{i \rightarrow j}^{0 \rightarrow 1} &= P[s_j(t+1) = 1, i \rightarrow j | s_i(t) = 1, s_j(t) = 0] \\ &= P_i^j \cdot P_{i \rightarrow j}, \end{aligned} \quad (1)$$

where $P_i^j = P[s_j(t+1) = 1 | s_i(t) = 1, s_j(t) = 0]$ in Eq. (1) is the probability of $s_j(t+1) = 1$ under the conditions $s_i(t) = 1$ and $s_j(t) = 0$, and the quantity $P_{i \rightarrow j} = P[i \rightarrow j | s_i(t) = 1, s_j(t) = 0, s_j(t+1) = 1]$ is the posteriori probability of $i \rightarrow j$ given $s_i(t) = 1$, $s_j(t) = 0$ and $s_j(t+1) = 1$.

To illustrate how the value of P_i^j can be calculated from matrix S , we consider an illustrative example. Say we know that, at time $t=1, 5, 8$ and 10 , the state of node i is in an active state [i.e., $s_i(t) = 1$, for $t=1, 5, 8, 10$] and state of node j is in an inactive state [i.e., $s_j(t) = 0$, for $t=1, 5, 8, 10$]. From the matrix S , we have $s_j(t=2) = 1$, $s_j(t=6) = 1$, $s_j(t=9) = 1$, and $s_j(t=11) = 0$. We get $P_i^j = 3/4$.

Take the network in Fig. 1(a) as an example. If we wish

to infer the neighbors of node 33, we can extract some pairs of time strings, as shown in Fig. 1(b), where each pair includes the time string with $s_{33}(t) = 0$ and its next time strings (i.e., at $t + 1$). We see that four pairs of such time strings can be extracted: T and $T + 1$, $T + 1$ and $T + 2$, $T + 5$ and $T + 6$, $T + 7$ and $T + 8$, where each pair is highlighted by frames with a different color. Based on these time strings, we can calculate P_i^{33} for all $i \neq j$. For example, we have $P_{16}^{33} = 2/3$, as shown in Fig. 1(b). Our goal is then to exploit statistical inference to estimate the posterior probability $P_{i \rightarrow j}$. Node i is a neighbor of node j if $P_{i \rightarrow j} > 0$, otherwise, $P_{i \rightarrow j} = 0$ if they are not connected. This analysis indicates that the values of P_i^j and $P_{i \rightarrow j}$ do not depend on time, so the probability $P[s_j(t + 1) = 1, i \rightarrow j | s_i(t) = 1, s_j(t) = 0]$ can simply be denoted as $P_{i \rightarrow j}^{0 \rightarrow 1}$, which does not depend on time either.

Remark 1. For the Markovian type of dynamical processes considered, the probability of each node's being activated is affected *only* by its *active* neighbors. Other scenarios require a generalization of our method to non-Markovian type of dynamics.

Remark 2. To reconstruct the network structure from time series data, a necessary condition is that the network structure should have detectable effects on the dynamics. If the dynamical processes are independent of the network structure, the reconstruction task is impossible. For the dynamical processes studied, the probability of each node's being activated is affected *only* by its *active* neighbors.

A non-zero value of the probability P_i^j indicates that node j is affected by node i . Since the probability of each node's being activated is determined solely by its active neighbors, a non-zero value of P_i^j indicates an actual connection between node i and j , which does not depend on time. The value of $P_{i \rightarrow j}$ can be estimated once the matrix S is given, which does not depend on time either. As a result, the probability in Eq. (1) can be denoted as $P_{i \rightarrow j}^{0 \rightarrow 1}$. From Eq. (1), we see that, if node j is not activated at time t_m , the expected number of node j being activated by its neighbors at $t_m + 1$ is given by

$$\begin{aligned} E_j^{t_m+1} &= \sum_{i \neq j} P_{i \rightarrow j}^{0 \rightarrow 1} \Psi_i^{t_m} + \varepsilon_j \\ &= \sum_{i \neq j} P_{i \rightarrow j} \cdot P_i^j \Psi_i^{t_m} + \varepsilon_j, \end{aligned} \quad (2)$$

where $\Psi_i^{t_m} = 1$ when node i was activated at time t_m , otherwise, $\Psi_i^{t_m} = 0$. ε_j characterizes the stochastic influence (noise) on node j .

Note that, due to the errors from the collected data and the assumptions used in the development of the method (e.g., the assumption of the Poisson distribution), it is necessary to consider the presence of noise perturbation in Eq. (2). While different types of noise can be considered, additive noise facilitates both computation and analysis, as done in previous works (e.g., Ref. [43]).

To simplify notation, we let Θ denote the quantities $P_{i \rightarrow j}$ and ε_j . To derive analytically an EM estimation, we assume that the relevant probability distributions are Poisson [58, 59]. The reason is that Poisson distribution can be generally used to characterize the probability of a given number of events occurring in a fixed interval of time. It is thus natural to use Poisson distribution to describe the *times* that node i being activated. As in Refs. [59, 62–64], using the Poisson distribution can make feasible mathematical analysis and computations with the EM algorithm (described below). We note that, with any assumption of the probability distribution, errors are inevitable. For example, the value of $P_{i \rightarrow j}$ may be slightly larger than zero even though node i is not a neighbor of node j . To reduce such errors, a remedy is to set a cutoff threshold to determine if $P_{i \rightarrow j} > 0$ indicates an actual link or it is simply an error.

The probability Ψ_j can then be expressed as

$$P\left(\{\Psi_j^{t_m+1}\}_{m=1, \dots, M} \mid \Theta, \{\Psi_i^{t_m}\}_{m=1, \dots, M; i=1, \dots, N}\right) = \prod_{m, \Psi_j^{t_m}=0} \frac{e^{-E_j^{t_m+1}} (E_j^{t_m+1})^{\Psi_j^{t_m+1}}}{\Psi_j^{t_m+1}!} \quad (3)$$

Next, we exploit the EM method to maximize the likelihood Eq. (3) so that the model parameters Θ can be estimated from the binary data. The EM algorithm is general for finding the maximum likelihood estimate in latent variable models, which contains two steps. For the E-Step, one “fills in” the latent variables using the posterior probability and, for the M-Step, one maximizes the expected complete logarithmic likelihood with respect to the complete posterior distribution. Jensen's inequality is a key tool in the M-step for generating the EM objective function. A comprehensive explanation of the principle of EM algorithm can be found in Ref. [65]. The algorithm has also been widely used in network structure reconstruction, e.g., in Refs. [59, 62–64]. It is convenient to maximize the logarithm of the likelihood:

$$\begin{aligned} L(\Theta) &= \sum_{m, \Psi_j^{t_m}=0} \left[\Psi_j^{t_m+1} \log \left(\sum_{i \neq j} P_{i \rightarrow j} P_i^j \Psi_i^{t_m} + \varepsilon_j \right) \right. \\ &\quad \left. - \left(\sum_{i \neq j} P_{i \rightarrow j} P_i^j \Psi_i^{t_m} + \varepsilon_j \right) \right], \end{aligned} \quad (4)$$

$\Psi_j^{t_m+1}! \equiv 1$ since $\Psi_j^{t_m+1}$ equals 0 or 1 in this work, therefore we have omitted the terms $\Psi_j^{t_m+1}!$. Using

Jensen's inequality [66], we obtain

$$\begin{aligned}
& \log \left(\sum_{i \neq j} P_{i \rightarrow j} P_i^j \Psi_i^{t_m} + \varepsilon_j \right) \\
&= \log \left(\sum_{i \neq j} \rho_i^{t_m} \frac{P_{i \rightarrow j} P_i^j \Psi_i^{t_m}}{\rho_i^{t_m}} + \rho_\varepsilon^{t_m} \frac{\varepsilon_j}{\rho_\varepsilon^{t_m}} \right) \\
&\geq \sum_{i \neq j} \rho_i^{t_m} \log \frac{P_{i \rightarrow j} P_i^j \Psi_i^{t_m}}{\rho_i^{t_m}} + \rho_\varepsilon^{t_m} \log \frac{\varepsilon_j}{\rho_\varepsilon^{t_m}} \\
&= \sum_{i \neq j} \rho_i^{t_m} \log P_{i \rightarrow j} P_i^j \Psi_i^{t_m} + \rho_\varepsilon^{t_m} \log \varepsilon_j \\
&- \sum_{i \neq j} \rho_i^{t_m} \log \rho_i^{t_m} - \rho_\varepsilon^{t_m} \log \rho_\varepsilon^{t_m}, \tag{5}
\end{aligned}$$

where

$$\rho_i^{t_m} = \frac{P_{i \rightarrow j} P_i^j \Psi_i^{t_m}}{\sum_{i' \neq j} P_{i' \rightarrow j} P_{i'}^j \Psi_{i'}^{t_m} + \varepsilon_j} \tag{6}$$

and

$$\rho_\varepsilon^{t_m} = \frac{\varepsilon_j}{\sum_{i' \neq j} P_{i' \rightarrow j} P_{i'}^j \Psi_{i'}^{t_m} + \varepsilon_j}. \tag{7}$$

To find a maximum likelihood solution of Eq. (4), we seek to maximize the following quantity:

$$\begin{aligned}
L(\Theta, \rho) &= \sum_{m, \Psi_j^{t_m}=0} \sum_{i \neq j} \left(\Psi_j^{t_m+1} \rho_i^{t_m} \log P_{i \rightarrow j} P_i^j \Psi_i^{t_m} \right. \\
&- \Psi_j^{t_m+1} \rho_i^{t_m} \log \rho_i^{t_m} - P_{i \rightarrow j} P_i^j \Psi_i^{t_m} \left. \right) + \\
&\sum_{m, \Psi_j^{t_m}=0} \left[\Psi_j^{t_m+1} \rho_\varepsilon^{t_m} \log \varepsilon_j - \Psi_j^{t_m+1} \rho_\varepsilon^{t_m} \log \rho_\varepsilon^{t_m} - \varepsilon_j \right] \tag{8}
\end{aligned}$$

with respect to Θ and ρ . Calculating the partial derivative of $L(\Theta, \rho)$ with respect to $P_{i \rightarrow j}$ and ε_j and setting them to be zero, we have

$$\frac{\partial L(\Theta, \rho)}{\partial P_{i \rightarrow j}} = \sum_{m, \Psi_j^{t_m}=0} \left(\frac{\Psi_j^{t_m+1} \rho_i^{t_m}}{P_{i \rightarrow j}} - P_i^j \Psi_i^{t_m} \right) = 0 \tag{9}$$

and

$$\frac{\partial L(\Theta, \rho)}{\partial \varepsilon_j} = \sum_{m, \Psi_j^{t_m}=0} \left(\frac{\Psi_j^{t_m+1} \rho_\varepsilon^{t_m}}{\varepsilon_j} - 1 \right) = 0, \tag{10}$$

which give

$$P_{i \rightarrow j} = \frac{\sum_{m, \Psi_j^{t_m}=0} (\Psi_j^{t_m+1} \rho_i^{t_m})}{\sum_{m, \Psi_j^{t_m}=0} (P_i^j \Psi_i^{t_m})} \tag{11}$$

and

$$\varepsilon_j = \frac{\sum_{m, \Psi_j^{t_m}=0} (\Psi_j^{t_m+1} \rho_\varepsilon^{t_m})}{\sum_{m, \Psi_j^{t_m}=0} (1)}, \tag{12}$$

respectively.

Equations (6), (7), (11) and (12) constitute our method. From the initial conditions of $P_{i \rightarrow j}$ and ε_j , we can iterate these equations until convergence is achieved. Since a single iterative process does not ensure global optimization, we carry out the above iteration process several times and choose the relevant values that give the maximum of the quantity in Eq. (4). As an example, Fig. 1(c) shows the value of $P_{i \rightarrow 33}$ (only $P_{i \rightarrow 33} > 0$ is shown) calculated from the iterative process. Similarly, the values of $P_{i \rightarrow j}$ for all the nodal pairs can be calculated, as shown in Fig. 1(d), where the red and blue dots denote the actual and non-existent links, respectively. Theoretically, node i is a neighbor of node j if $P_{i \rightarrow j} > 0$ with the threshold value $\Delta = 0$. However, the simple choice of $\Delta = 0$ will lead to error due to the uncertain factors. For example, as shown in Fig. 1(e), there are eight false links (represented by the red lines). In this case, it is necessary to choose a non-zero threshold for each node to eliminate reconstruction error. For instance, by setting $\Delta = 1/N$ for all nodes in Fig. 1, we can reconstruct the original network with zero error.

An explanation is in order. It is often difficult to directly maximize the formula in Eq. (4). We can first use Jensen's inequality to get the lower bound of the formula at Θ , which is denoted by $L^-(\Theta) = \sum_{i \neq j} \rho_i^{t_m} \log P_{i \rightarrow j} P_i^j \Psi_i^{t_m} + \rho_\varepsilon^{t_m} \log \varepsilon_j - \sum_{i \neq j} \rho_i^{t_m} \log \rho_i^{t_m} - \rho_\varepsilon^{t_m} \log \rho_\varepsilon^{t_m}$ - the last term of Eq. (5). We initialize the parameter Θ_1 , e.g., by setting $P_{1 \rightarrow j} = P_{j-1 \rightarrow j} = P_{j+1 \rightarrow j} = \dots, P_{N \rightarrow j} = \varepsilon_j = 1/N$. We can show that the equality conditions in Eq. (8) are satisfied when the conditions in Eqs. (6) and (7) are met. We thus have $L_{\Theta_1}^-(\Theta_1) = L(\Theta_1)$, where $L_{\Theta_1}^-(\Theta)$ denotes the lower bound function of $L(\Theta)$ at Θ_1 , so $L_{\Theta_1}^-(\Theta_1)$ indicates the value of $L_{\Theta_1}^-(\Theta)$ at $\Theta = \Theta_1$. Further, by maximizing $L_{\Theta_1}^-(\Theta)$, we obtain a new maximum point Θ_2 :

$$L(\Theta_2) \geq L_{\Theta_1}^-(\Theta_2) \geq L_{\Theta_1}^-(\Theta_1) = L(\Theta_1),$$

meaning that Θ_2 is a better solution than Θ_1 .

We also note that the initial conditions of $P_{i \rightarrow j}$ and ε_j can be chosen in different ways. For example, we can set $P_{1 \rightarrow j} = P_{j-1 \rightarrow j} = P_{j+1 \rightarrow j} = \dots, P_{N \rightarrow j} = \varepsilon_j = 1/N$. The quantities $\rho_i^{t_m}$ and $\rho_\varepsilon^{t_m}$ in Eqs. (6) and (7) can be calculated, guaranteeing the equality condition in Eq. (8). Then, Eqs. (11) and (12) can be calculated. Iterating the above process leads to a local optimal solution. The value of the likelihood function at the next time step is better than that at the last step. Since the convergence of the EM algorithm has been confirmed in many previous

works, we can stop the iteration process when the value of the likelihood function is stable or the fluctuations are smaller than a given threshold value. While one round of the iteration may yield a local rather than a global optimal solution, we can choose different sets of initial values to carry out different rounds of iteration and choose the best solution.

We remark that errors in the collected data and uncertainties in the assumption of the Poisson distribution can be modeled by noise perturbation. The simple choice of Δ will lead to small errors. While errors cannot be completely eliminated by increasing the value of M , the gap that is key to distinguishing actual from non-existent links will be enlarged. Figure 1 shows that the accuracy of reconstruction can be improved if we set $\Delta = 1/N$ for all nodes.

III. PERFORMANCE CHARACTERIZATION AND DEMONSTRATION

A. Local and global performance indicators

We use a number of indicators to characterize the local and global performance of our reconstruction methodology.

AUROC and AUPR - local performance indicators. The AUROC (area under receiver operating characteristic, δ_{AUROC}) and AUPR (area under precision-recall, δ_{AUPR}) curves are standard local (node-wise) performance indicators used widely in signal processing and computer science [67], which can be calculated for each node in the network. The average values over all the nodes can then be used to characterize the reconstruction performance for the whole network. To define AUROC and AUPR, it is necessary to calculate three basic quantities: TPR (true positive rate, R_{TP}), FPR (false positive rate, R_{FP}), and Recall. In particular, TPR is defined as

$$R_{TP}(l) = \frac{P_T(l)}{P}, \quad (13)$$

where l is the cutoff in the list of reconstructed links, $P_T(l)$ is the number of true positives in the top l predictions in the link list, and P is the number of positives. FPR is given by

$$R_{FP}(l) = \frac{P_F(l)}{Q}, \quad (14)$$

where $P_F(l)$ is the number of false positive in the top l predictions in the link list, and Q is the number of negatives in the gold standard. The reconstruction precision can be defined as

$$\delta_{Precision}(l) = \frac{P_T(l)}{P_T(l) + P_F(l)} = \frac{P_T(l)}{l}. \quad (15)$$

The measure Recall is defined as

$$\delta_{Recall}(l) = R_{TP}(l) = \frac{P_T(l)}{P}. \quad (16)$$

Varying the value of l from 0 to N , we plot two sequences of points: $[R_{FP}(l), R_{TP}(l)]$ and $[\delta_{Recall}(l), \delta_{Precision}(l)]$. The areas under the two curves give the values of AUROC and AUPR, respectively. For the case of zero error in reconstruction where all the actual links have been predicted, we have $\delta_{AUROC} = 1$ and $\delta_{AUPR} = 1$. In the worse case scenario where the predicted links are completely random (so that the reconstruction tasks fails entirely), we have $\delta_{AUROC} = 0.5$ and $\delta_{AUPR} = P/2N$.

F1 score - a global performance indicator. Higher values of AUROC and AUPR *only* demonstrate that the prediction of the actual links are better than that for the non-existent links, but do not give the number of actual links in the network. These local measures do not indicate whether a specific link has been correctly inferred. To determine whether a reconstructed probability value (i.e., $P_{i \rightarrow j}$) corresponds to an actual or a null link, it is necessary to set a threshold Δ for each node. Figure 2 shows, for each node, the value of $P_{i \rightarrow j}$ for $i \neq j$ ($i = 1, 2, \dots, N$) in three model networks: random network (ER) [68], scale-free network (BA or SF) [69], and small-world (SW) network [70]. The dynamical processes are Voter dynamics in Fig. 2(a) and Kirman dynamics in Fig. 2(b)), respectively. (The details of these two processes, together with other six other types, are given in Appendix.) We see that, for node j , there exists a gap dividing the values of $P_{i \rightarrow j}$ for $i \neq j$ ($i = 1, 2, \dots, N$). It is thus reasonable to place a threshold Δ_j in the gap for node j to determine whether a value of $P_{i \rightarrow j}$ can be regarded as representing an actual links (red points, $P_{i \rightarrow j} > \Delta_j$) or a non-existent link (blue points, $P_{i \rightarrow j} < \Delta_j$). In so doing, we obtain the nonzero values $P_{i \rightarrow j} > 0$ for $i \neq j$ and re-rank them in a descending order, denoted as P'_l ($l = 1, 2, \dots$).

It is important to choose a proper threshold Δ_j for each node j . From Fig. 2, we see that there is a gap, which can be used to separate the actual from the non-existent links. Computationally, it is necessary to set a threshold for the task. We consider two different scenarios. First, suppose that a sequence of the values of $P_{i \rightarrow j}$ is 0.8, 0.7, 0.6, 0.01, and 0.0001. In this case, the threshold can be set between the values of 0.6 and 0.01 through the maximum value of $P'_l - P'_{l+1}$. However, the threshold value is between 0.01 and 0.0001 when using P'_l/P'_{l+1} . For this scenario, the former choice of the threshold value is more reasonable than the latter. Second, for a different sequence, such as 0.2, 0.1, 0.09 and 0.0001, through $P'_l - P'_{l+1}$ we find a threshold value between 0.2 and 0.1. However, through P'_l/P'_{l+1} , we get a threshold value between 0.09 and 0.0001. For this scenario, the latter case is more reasonable. Combining the two cases, we define the threshold Δ_j for node j as

$$\Delta_j = \arg \max_l \left[\frac{P'_l}{P'_{l+1}} (P'_l - P'_{l+1}) \right]. \quad (17)$$

With the threshold value so determined, we can ascertain, for any pair of nodes in the network, whether there

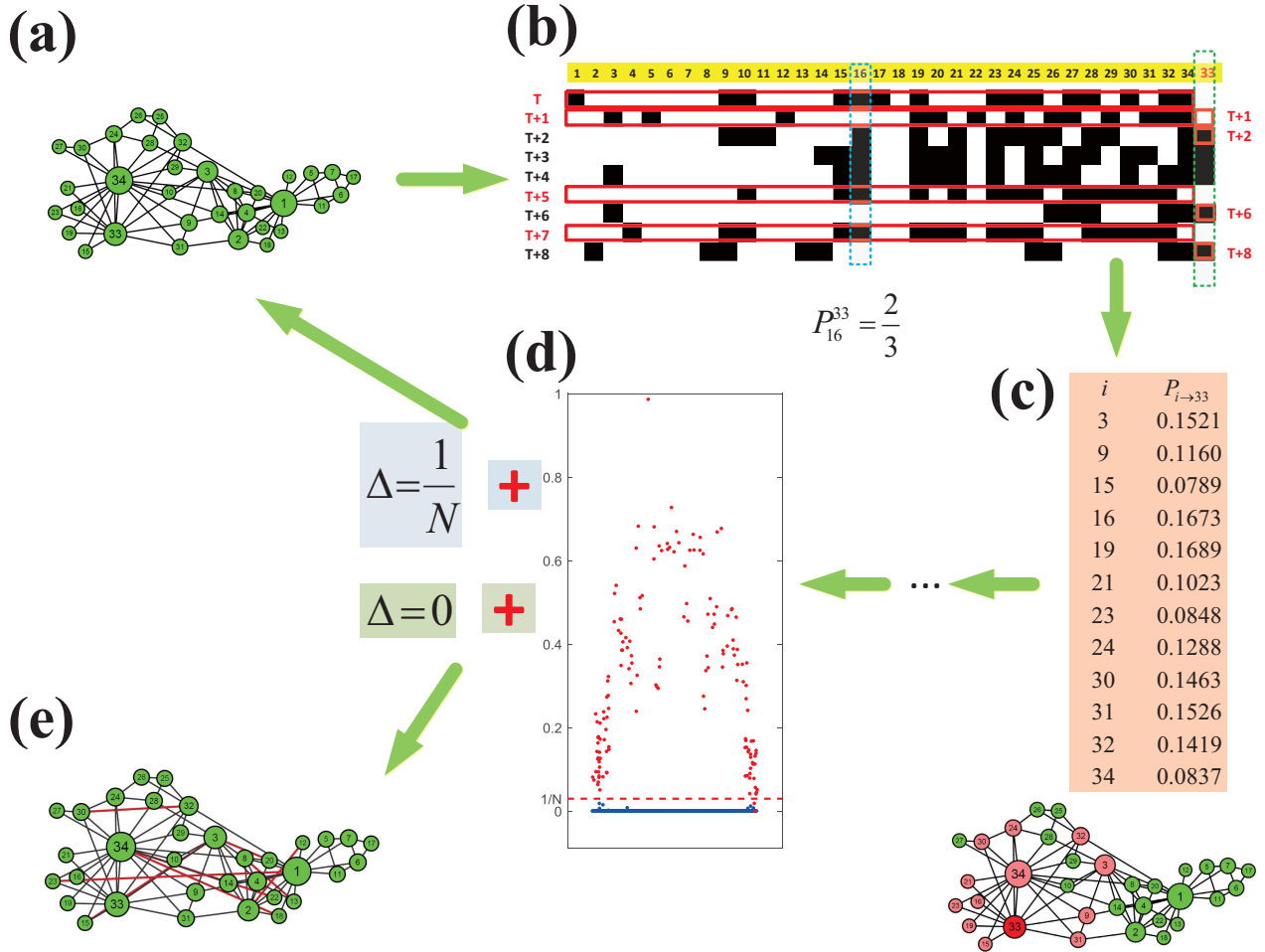


FIG. 1. **Schematic illustration of our binary-state network reconstruction methodology based on statistical inference.** In this example, the data are collected by implementing the voter model on an empirical network - the Zachary karate-club network, where initially 30% of the nodes are randomly set to state 1. (a) The actual structure of the network. (b) The data matrix, where each row is a time string representing all nodes' states at that time step and each column is a node's state at different time steps. The black and blank squares denote the 1 and 0 state, respectively. Say we wish to ascertain all neighbors of node 33 (highlighted by the red frame), so only the strings with $\Psi_{33}^t = 0$ and its next string at $t + 1$ are used. Each pair of useful strings are highlighted by a frame with a different color. The quantity P_{16}^{33} is the probability of the event $s_{33}(t + 1) = 1$ under the prior conditions of $s_{16}(t) = 1$ and $s_{33}(t) = 0$. We have $P_{16}^{33} = 2/3$ for this example (highlighted by the blue frame). (c) The values of $P_{i \rightarrow 33}$ are obtained through the EM algorithm, where only the non-zero values of the probability are shown. The neighbors of node 33 in the network are shown in the lower right corner (marked by light red color). (d) The values of $P_{i \rightarrow j}$ for each node j , where the red nodes and blue points denote the actual and non-existent links, respectively. The red dashed line represents the threshold $\Delta = 1/N$ for determining whether a reconstructed value $P_{i \rightarrow j}$ can be regarded as representing an actual link or a null link. (e) If we choose $\Delta = 0$, there are eight false links as predicted (marked by the red links in the network). However, for $\Delta = 1/N$, all actual links are correctly inferred.

is an actual link. The F1 score is given by [71];

$$F1 = \frac{2\delta_{Precision}\delta_{Recall}}{\delta_{Precision} + \delta_{Recall}}, \quad (18)$$

where $\delta_{Precision} = P_T/(P_T + P_F)$ and $\delta_{Recall} = P_T/(P_T + N_F)$ respectively. The quantities P_T , N_F , P_F and N_T denote the true positive, false negative, false positive and true negative. The condition $F1 = 1$ indicates that the reconstructed links perfectly match with those in the

original network.

Another global indicator, denoted by $ERR(R_{ER})$, is defined as the ratio of the number of erroneous links (false positive and false negative) to the number of links of the true network. Namely,

$$R_{ER} = \frac{N_F + P_F}{P_T + N_F}. \quad (19)$$

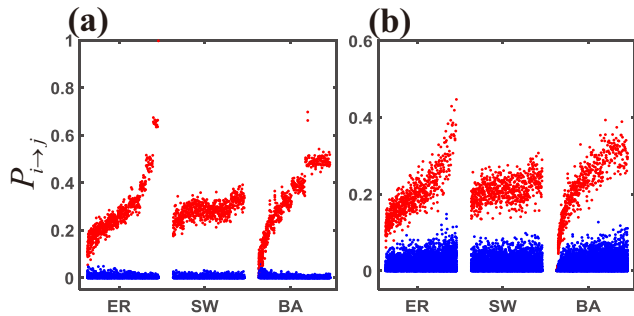


FIG. 2. **Demonstration of placement of threshold probability value for calculating the global performance indicator F1.** For combinations of two types of binary-state dynamics [voter dynamics in (a) and Kirman dynamics in (b)] and three complex network topologies, the values of $P_{i \rightarrow j}$ for $i \neq j$ ($i = 1, 2, \dots, N$) for each node in the network are shown. The result for a node corresponds to a column above the x-axis consisting of $N - 1$ number of points. The red nodes and blue points denote the actual and non-existent links, respectively. Three model networks (ER, SW and SF networks) are used. All networks have $N = 100$ nodes and average degree $\langle k \rangle = 6$. The length of the binary time series is $M = 15000$.

B. Reconstruction performance with model and real networks

We consider eight types of binary-state dynamical processes as studied recently in Ref. [43] with the lasso method. For the network structures, we use three types of model complex networks (ER, SF, and WS) and a number of empirical networks as described in Appendix. In Tab. I, we compare the performance of our EM algorithm with that of the lasso method under the same setting. We see that the performances of the two methods for the threshold dynamics are almost identical as both exhibit nearly perfect values of AUROC and AUPR (almost 100%). However, for the other seven types of binary-state dynamics in combination with different network structures (model or empirical networks), our EM based reconstruction method yields results that are more accurate than those with the lasso method. The value of F1 scores from our method for various combinations of network structures and binary-state dynamics are summarized in Tab. II, where we see that the values of F1 score in most cases are close to unity, indicating accurate reconstruction performance. Since the lasso method does not rely on any threshold value for each node [43], it is not feasible to compare performance in terms of the F1 score.

Figure 3 shows, for the model networks, the dependence of the values of AUROC and F1 score on M , the length of the binary time series, where we see that, in all cases, AUROC approaches a stable and large (e.g., > 0.97) value for $M \approx 25000$. The values of F1 score are also large (e.g., > 0.92). In terms of the network topol-

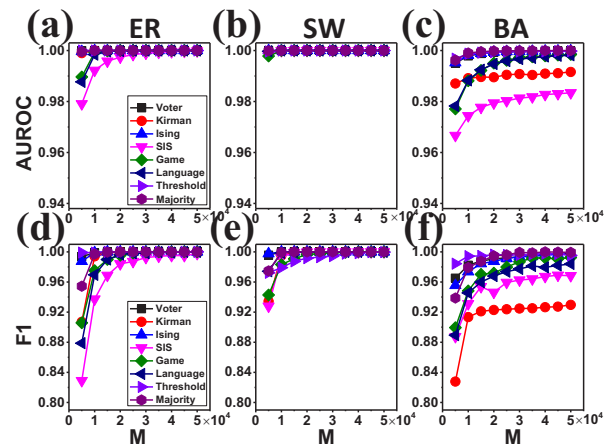


FIG. 3. **Dependence of reconstruction performance on data length.** For the eight types of binary-state dynamics implemented on ER, SW, and SF networks, AUROC (a-c) and F1 score (d-f) versus M , the length of the binary time series, for ER (left panel), SW (central panel), and SF (right panel) networks. All networks have $N = 500$ nodes with the average degree $\langle k \rangle = 6$. The parameters for each type of dynamics are described in Appendix. For the large number of combinations of binary dynamical processes and network topologies, both the local (AUROC) and global (F1 score) performance measures approach almost the highest possible values when M becomes sufficiently large.

ogy, the highest performance is achieved for the SW, followed by ER and then SF networks. The intuitive reason for the relatively inferior performance with SF networks lies in the difficulty to infer the neighbors of hub or high degree nodes.

Figure 4 shows results, for the combinations of eight binary dynamical processes and the three distinct complex network topologies, the dependence of the reconstruction performance on the network average degree $\langle k \rangle$. We note a decreasing trend in the reconstruction accuracy as the average degree becomes larger. The reason is that an increase in $\langle k \rangle$ demands more links to be predicted, leading to a decrease in the reconstruction accuracy if the data length is not increased accordingly. Another phenomenon is that, except for the SIS and Kirman dynamics, the average degree does not have an appreciable effect on the reconstruction accuracy. The heuristic reason of the relatively stronger dependence of the reconstruction performance on the average degree for the SIS and Kirman dynamics is that, for these two types of dynamics, the probability of being activated is proportional to the number of active neighbors m rather than the density of the active neighbors, m/k . As a result, increasing the average degree will expedite the dynamical propagation of the “virus” or information, leading to most nodes being activated in relatively short time. From the standpoint of reconstruction, this is damaging due to lack of sufficient information about the time evolution of the underlying dynamics. To improve the reconstruction performance,

TABLE I. **Local reconstruction performance with model and real networks.** Values of AUROC and AUPR for various dynamics on a variety of model and empirical (real) networks. The parameters in the dynamical models are described in Appendix. The size and average degree of the three types of model complex networks (ER, BA, and SW) are $N = 500$ and $\langle k \rangle = 6$. The length of the binary data string is $M = 50000$ for $N = 500$, $M = 15000$ for $N < 500$, and $M = 100000$ for $N > 1000$. The largest values AUROC and AUPR for each case is highlighted in bold. For comparison, the corresponding AUROC and AUPR values from the recent lasso method [43] are also shown.

AUROC/AUPR		Voter	Kirman	Ising	SIS	Game	Language	Threshold	Majority
Karate	lasso	0.980/0.971	0.990/0.959	0.997/0.997	0.954/0.946	0.993/0.992	0.961/0.926	0.995/0.996	0.997/0.996
	EM	0.999/0.999	1.000/1.000	1.000/1.000	0.983/0.982	1.000/1.000	0.998/0.998	1.000/1.000	1.000/1.000
Dolphins	lasso	0.974/0.917	0.996/0.984	0.999/0.997	0.981/0.941	0.996/0.988	0.987/0.945	1.000/1.000	0.998/0.992
	EM	1.000/1.000	1.000/1.000	1.000/1.000	0.998/0.993	1.000/1.000	1.000/0.999	1.000/0.999	1.000/1.000
Polbooks	lasso	0.967/0.865	0.984/0.912	0.989/0.968	0.896/0.801	0.974/0.926	0.951/0.851	1.000/0.999	0.983/0.943
	EM	1.000/0.999	1.000/1.000	1.000/0.999	0.940/0.864	0.994/0.991	0.991/0.975	0.998/0.998	0.999/0.997
Football	lasso	0.959/0.812	0.991/0.949	0.991/0.950	0.928/0.711	0.986/0.920	0.927/0.703	1.000/1.000	0.987/0.927
	EM	1.000/1.000	1.000/1.000	1.000/1.000	0.996/0.973	0.999/0.998	0.999/0.994	1.000/1.000	1.000/0.999
Email	lasso	0.943/0.781	0.655/0.331	0.971/0.808	0.789/0.607	0.968/0.860	0.923/0.622	1.000/0.998	0.965/0.723
	EM	1.000/1.000	0.955/0.799	1.000/1.000	0.977/0.893	0.999/0.997	0.999/0.990	1.000/1.000	1.000/1.000
ER(500)	lasso	0.999/0.975	0.988/0.784	0.998/0.974	0.994/0.972	0.999/0.979	0.977/0.751	1.000/1.000	0.996/0.929
	EM	1.000/1.000	1.000/1.000	1.000/1.000	1.000/0.997	1.000/1.000	1.000/1.000	1.000/1.000	1.000/1.000
SW(500)	lasso	1.000/1.000	0.992/0.838	1.000/0.998	1.000/1.000	1.000/0.998	0.997/0.930	1.000/1.000	0.998/0.937
	EM	1.000/1.000	1.000/1.000	1.000/1.000	1.000/1.000	1.000/1.000	1.000/1.000	1.000/1.000	1.000/1.000
BA(500)	lasso	0.996/0.953	0.940/0.697	0.994/0.963	0.968/0.926	0.989/0.946	0.978/0.861	1.000/0.998	0.994/0.944
	EM	1.000/0.999	0.992/0.971	1.000/1.000	0.983/0.949	0.998/0.997	0.998/0.992	1.000/1.000	1.000/1.000

TABLE II. **Characterization of global performance of proposed statistical inference based reconstruction method.** Listed are the values of F1 score and ERR for various combinations of binary dynamics and networks (model and empirical), where the threshold Δ_j for each node is determined according to Eq. (17). Other parameters are the same as in Tab. I.

F1/ERR	Voter	Kirman	Ising	SIS	Game	Language	Threshold	Majority
Karate	0.994/0.013	1.000/0.000	1.000/0.000	0.981/0.039	0.994/0.013	1.000/0.000	0.947/0.103	1.000/0.000
Dolphins	1.000/0.000	1.000/0.000	0.997/0.006	0.984/0.031	0.994/0.013	1.000/0.000	1.000/0.000	0.994/0.013
polbooks	0.986/0.027	1.000/0.000	0.990/0.020	0.867/0.254	0.972/0.054	0.960/0.077	0.986/0.027	0.972/0.057
Football	1.000/0.000	0.999/0.002	0.999/0.002	0.844/0.277	0.992/0.015	0.941/0.116	0.963/0.072	0.992/0.016
Email	0.998/0.004	0.712/0.531	0.998/0.004	0.853/0.265	0.984/0.031	0.943/0.108	0.995/0.010	1.000/0.001
ER(500)	1.000/0.000	1.000/0.000	1.000/0.000	0.998/0.005	1.000/0.000	1.000/0.000	1.000/0.000	1.000/0.000
SW(500)	1.000/0.000	1.000/0.000	1.000/0.000	1.000/0.000	1.000/0.000	1.000/0.000	1.000/0.000	1.000/0.000
BA(500)	0.998/0.006	0.930/0.142	0.997/0.008	0.968/0.064	0.993 /0.016	0.984/0.033	0.995/0.011	0.999/0.003

one can reduce the transmission rate λ in the SIS process and the transmission rate $c_1 + md$ in the Kirman dynamics. On the contrary, for other six types of binary-state dynamics, for a large average degree value, the probability of being activated is not significantly increased due to its dependence on the density m/k (not on m itself), so the slow pace of the dynamical evolution on the networks persists and, consequently, there is still sufficient amount of information required for the reconstruction task.

Finally, we demonstrate the robustness of our EM algorithm against stochastic disturbance. Specifically, we randomly flip a fraction ρ of the binary states among the total number MN of states and calculate the values of AUROC and F1 score versus ρ for various combinations of the dynamics and network topology. The results are shown in Fig. 5. From the top panel, we see that the values of AUROC are larger than 0.96 even when 20% of the states are flipped, which are more robust than those with the lasso method (e.g., Tab. 3 in Ref. [43]). We also see that the reconstruction performances with the voter and threshold dynamics are relatively more robust to stochastic perturbations than those with the other six

types of dynamical processes. A possible reason is that, in the game dynamics, each node’s payoff depends sensitively on the neighbors’ states. If one neighbor’s state is flipped, there can be a dramatic change in the payoff, affecting directly its strategy (cooperation or defection) and consequently the reconstruction accuracy.

IV. DISCUSSION

In physics and mathematics, the various inverse problems to infer the internal structure or “gears” of the underlying system based on observations are always challenging. For complex networked systems, recent years have witnessed the development of various frameworks and methodologies to address the inverse or reverse-engineering problem [51], leading to the gradual establishment of a “toolbox” of network and dynamics reconstruction algorithms to deal with a variety of specific tasks. This work adds another piece into this toolbox: a statistical inference based method specifically designed to address the network reconstruction problem for bi-

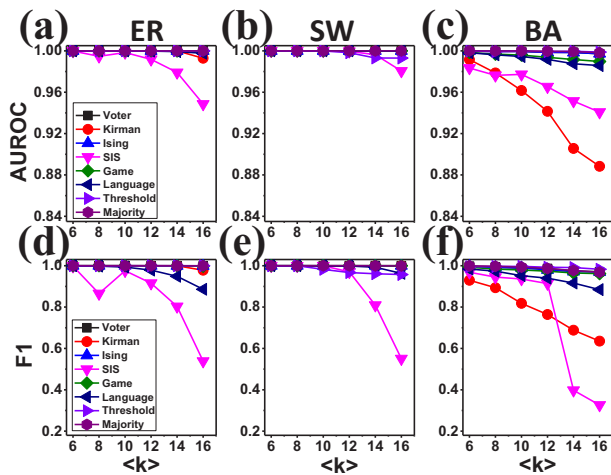


FIG. 4. **Effect of increasing the network average degree on reconstruction performance.** For the eight types of binary-state dynamics implemented on ER, SW, and SF networks, AUROC (a-c) and F1 score (d-f) versus the average degree $\langle k \rangle$, for ER (left panel), SW (central panel), and SF (right panel) networks. All networks have $N = 500$ nodes and the length of the binary time series is fixed at $M = 50000$. In general, the reconstruction accuracy tends to decrease as the average degree becomes larger.

nary dynamical processes without requiring any *a priori* knowledge about the switching functions generating the binary-state dynamics. The key underpinning of our method is an expectation-maximization based algorithm to maximize the probability (likelihood) that there is a link between an arbitrary pair of nodes in the network. As a result, a feature that is particularly appealing from the standpoint of network reconstruction arises: a distinct gap between the probability values that correspond to actual links and those associated with non-existent links. Statistical inference theory also enables us to obtain an explicit formula for placing a threshold in the gap so that the actual and non-existent links can be distinguished unambiguously in an automated fashion. It is this feature that leads to the superior performance of our statistical inference based methodology as compared with those of the previous methods. In particular, we demonstrate, using a large number of combinations of binary dynamical processes and complex network topologies, that our method is capable of reconstructing the network structure based solely on binary time series with unprecedented accuracy, regardless of the nature of the intrinsic switching functions generating the binary state dynamics. Additional features of our methodology are effectively parameter free and robustness against stochastic fluctuations in the data. While our method is articulated for network structural reconstruction and hence does not address the issue of identifying the underlying dynamical processes, it represents a practically useful addition to the toolbox of reconstructing complex networks structure and dynamics, which is being expanded at a rapid

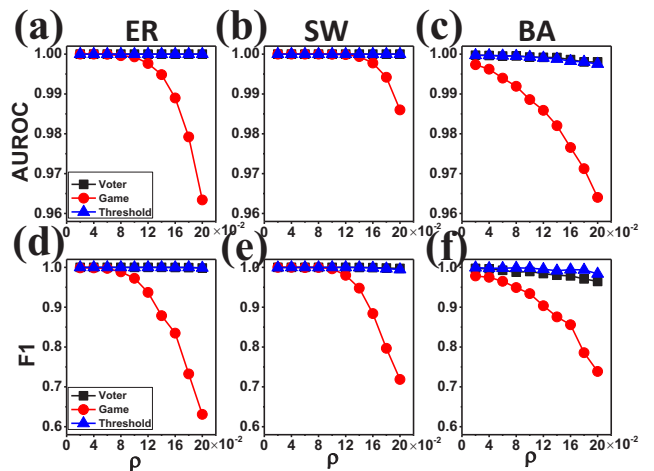


FIG. 5. **Effect of stochastic disturbance on reconstruction.** The local (AUROC, a-c) and global (F1 score, d-f) performance indicators versus ρ , the fraction of randomly flipped binary states in the data, for the voter (blue squares), game (red circles), and threshold (blue up triangles) models, for ER (left panel), SW (central panel), and SF (right panel) networks. All networks have the size $N = 500$ with the average degree $\langle k \rangle = 6$. The length of the binary time series is $M = 50000$.

pace by many research groups.

ACKNOWLEDGMENTS

The authors thank Dr. Z.-S. Shen for discussions. This work was supported by NSFC under Grant Nos. 61473001 and 11331009, and partially supported by the Young Talent Funding of Anhui Provincial Universities under Grant No. gxyqZD2017003. YCL would like to acknowledge support from the Vannevar Bush Faculty Fellowship program sponsored by the Basic Research Office of the Assistant Secretary of Defense for Research and Engineering and funded by the Office of Naval Research through Grant No. N00014-16-1-2828.

APPENDIX

The basic structural parameters of the five empirical networks used in the numerical demonstration are summarized in Tab. III. The eight binary-state dynamical modes are summarized below with parameters given in Ref. [43].

(1) *Voter model.* The voter model assumes that a node randomly chooses and then adopts one of its neighbors' state at each time step. If m neighbors among total k neighbors are in an active state, the probabilities of being active and inactive are m/k and $(k - m)/k$, respectively [72]. Since the voter model can cause the

TABLE III. **Structural parameters of the five empirical networks used in our numerical simulations.** The parameters N and E are the total numbers of nodes and links, respectively, C and r are the clustering and assortative coefficients, respectively, H is the degree heterogeneity defined as $H = \langle k^2 \rangle / \langle k \rangle^2$.

Network	N	E	$\langle k \rangle$	C	r	H
Karate	34	78	4.5882	0.5879	-0.4756	1.6933
Dolphins	62	159	5.129	0.2901	-0.0718	1.3255
Polbooks	105	441	8.40	0.4875	-0.1279	1.4207
Football	115	613	10.6609	0.4032	0.1624	1.0069
Email	1133	5451	9.6222	0.2540	0.0782	1.9421

nodal states to converge into a stable state, we randomly initialize the states of all nodes after each 100 time steps.

(2) *Kirman model.* In this model, each node changes its state from 0 to 1 with the probability $c_1 + dm$ and the probability associated with the opposite change is $c_2 + d(k - m)$, where the parameters c_1 and c_2 quantify the individual action that is independent of the states of the neighbors and d characterizes the action of copying from neighbors' state [73]. In our computations, we set $c_1 = 0.1$, $c_2 = 0.1$ and $d = 0.08$.

(3) *Ising model.* This is the classic paradigm for understanding ferromagnetism at the microscopic level of spins. Each node switches its state from 0 to 1 with the probability $[1 + e^{\beta(k-2m)/k}]^{-1}$ and from state 1 to 0 with the probability $[e^{\beta(k-2m)/k}]/[1 + e^{\beta(k-2m)/k}]$, where $\beta = 2$ characterizes the combining effect of temperature and ferromagnetic interaction [74].

(4) *SIS model.* This model describes the epidemic process of disease spreading with infection and recovery. A susceptible individual can be infected with probability $1 - (1 - \lambda)^m$ (from state 0 to 1) at each time step, and an infected node can recover to the susceptible state at the recovery rate μ , where λ is the transmission rate [52]. In our simulations, we set $\lambda = 0.5$ and $\mu = 0.5$ if the average degree is smaller than 10; otherwise we choose $\lambda = 0.35$ and $\mu = 0.5$.

(5) *Game model.* For evolutionary game dynamics on complex networks [54], a player (a node) can be a cooperator (active - the 1 state) or a defector (inactive - the 0 state). A player plays with each of his/her neighbors using one chosen strategy at every time step. The players obtain payoff a (d) if both choose to cooperate (defect). If one player cooperates while the other defects, the cooperator will obtain low payoff b , while the defector will gain higher payoff c . The payoff of a player is the sum of payoffs from playing game with all its neighbors. A player switches the strategy with a probability that depends on the payoff it may gain in the next round under the current circumstance. Each player switches its state from 0 to 1 with the probability $[\alpha + e^{\frac{\beta}{k}((a-c)(k-m)+(b-d)m)}]^{-1}$ and from state 1 to 0 with the probability $[\alpha + e^{\frac{\beta}{k}((c-a)(k-m)+(d-b)m)}]^{-1}$, where α qualifies the willingness for a player to change its strategy according to those of its neighbors, and β is associated with the effect of the expected payoff. We choose $a = b = 5$, $c = d = 0$, $\alpha = 0.1$, and $\beta = 1$ in our simulations.

(6) *Language model.* In this model, the two states denote two different language choices of a person. The transition probability from the primary to the secondary language is proportional to the fraction of speakers in the neighbors with the power α , multiplied by the parameter s (or $1 - s$) according to the respective language [75], where $\alpha = 0.7$ and $s = 0.5$. Because of the problem of converging to a stable state, we randomly initialize the states of all nodes after every 100 time steps.

(7) *Threshold model.* This is a deterministic model, where a node becomes active if the fraction of active neighbors m/k is larger than the threshold $1/2$, and no recovery transformation is permitted [76]. Due to the problem of fast convergence to a stable state from any initial condition, we randomly initialize the states of all nodes after every 5 time steps.

(8) *Majority-voter model.* In this model, a node tends to align with the majority state of its neighbors, with Q being the probability of misalignment [77]. We set $Q = 0.3$ and randomly initialize the states of all nodes after every 10 time steps to overcome the difficulty of fast convergence to a stable state.

-
- [1] S. Gruen, M. Diesmann, and A. Aertsen, *Neu. Comp.* **14**, 43 (2002).
[2] R. Gütig, A. Aertsen, and S. Rotter, *Neu. Comp.* **14**, 121 (2002).
[3] T. S. Gardner, D. di Bernardo, D. Lorenz, and J. J. Collins, *Science* **301**, 102 (2003).
[4] G. Pipa and S. Grün, *Neurocomp.* **52**, 31 (2003).
[5] A. Brovelli, M. Ding, A. Ledberg, Y. Chen, R. Nakamura, and S. L. Bressler, *Proc. Nat. Acad. Sci. (USA)* **101**, 9849 (2004).
[6] V. M. Eguiluz, D. R. Chialvo, G. A. Cecchi, M. Baliki, and A. V. Apkarian, *Phys. Rev. Lett.* **94**, 018102 (2005).
[7] D. S. Bassett, A. Meyer-Lindenberg, S. Achard, T. Duke, and E. Bullmore, *Proc. Nat. Acad. Sci. (USA)* **103**, 19518 (2006).
[8] D. Yu, M. Righero, and L. Kocarev, *Phys. Rev. Lett.* **97**, 188701 (2006).
[9] J. Bongard and H. Lipson, *Proc. Natl. Acad. Sci. (USA)* **104**, 9943 (2007).
[10] M. Timme, *Phys. Rev. Lett.* **98**, 224101 (2007).
[11] W. K.-S. Tang, M. Yu, and L. Kocarev, in *Circuits and Systems, ISCAS 2007. IEEE Inter. Symp.* (IEEE, 2007) pp. 2646–2649.

- [12] D. Napolitano and T. D. Sauer, *Phys. Rev. E* **77**, 026103 (2008).
- [13] E. Sontag, *Essays Biochem.* **45**, 161 (2008).
- [14] A. Clauset, C. Moore, and M. E. J. Newman, *Nature* **453**, 98 (2008).
- [15] W.-X. Wang, Q.-F. Chen, L. Huang, Y.-C. Lai, and M. Harrison, *Phys. Rev. E* **80**, 016116 (2009).
- [16] J. Donges, Y. Zou, N. Marwan, and J. Kurths, *EPL (Europhys. Lett.)* **87**, 48007 (2009).
- [17] J. Ren, W.-X. Wang, B. Li, and Y.-C. Lai, *Phys. Rev. Lett.* **104**, 058701 (2010).
- [18] J. Chan, A. Holmes, and R. Rabadan, *PLoS Comp. Bio.* **6**, e1001005 (2010).
- [19] Y. Yuan, G.-B. Stan, S. Warnick, and J. Goncalves, in *Decision and Control (CDC), 2010 49th IEEE Conference (IEEE, 2010)* pp. 810–815.
- [20] Z. Levnajić and A. Pikovsky, *Phys. Rev. Lett.* **107**, 034101 (2011).
- [21] S. Hempel, A. Koseska, J. Kurths, and Z. Nikoloski, *Phys. Rev. Lett.* **107**, 054101 (2011).
- [22] S. G. Shandilya and M. Timme, *New J. Phys.* **13**, 013004 (2011).
- [23] D. Yu and U. Parlitz, *PLOS ONE* **6**, e24333 (2011).
- [24] W.-X. Wang, Y.-C. Lai, C. Grebogi, and J.-P. Ye, *Phys. Rev. X* **1**, 021021 (2011).
- [25] W.-X. Wang, R. Yang, Y.-C. Lai, V. Kovanis, and C. Grebogi, *Phys. Rev. Lett.* **106**, 154101 (2011).
- [26] W.-X. Wang, R. Yang, Y.-C. Lai, V. Kovanis, and M. A. F. Harrison, *EPL (Europhys. Lett.)* **94**, 48006 (2011).
- [27] R. Yang, Y.-C. Lai, and C. Grebogi, *Chaos* **22**, 033119 (2012).
- [28] W. Pan, Y. Yuan, and G.-B. Stan, in *Decision and Control (CDC), 2012 IEEE 51st Annu. Conf. (IEEE, 2012)* pp. 2334–2339.
- [29] W.-X. Wang, J. Ren, Y.-C. Lai, and B. Li, *Chaos* **22**, 033131 (2012).
- [30] T. Berry, F. Hamilton, N. Peixoto, and T. Sauer, *J. Neurosci. Meth.* **209**, 388 (2012).
- [31] O. Stetter, D. Battaglia, J. Soriano, and T. Geisel, *PLoS Comp. Biol.* **8**, e1002653 (2012).
- [32] R.-Q. Su, X. Ni, W.-X. Wang, and Y.-C. Lai, *Phys. Rev. E* **85**, 056220 (2012).
- [33] R.-Q. Su, W.-X. Wang, and Y.-C. Lai, *Phys. Rev. E* **85**, 065201 (2012).
- [34] F. Hamilton, T. Berry, N. Peixoto, and T. Sauer, *Phys. Rev. E* **88**, 052715 (2013).
- [35] D. Zhou, Y. Xiao, Y. Zhang, Z. Xu, and D. Cai, *Phys. Rev. Lett.* **111**, 054102 (2013).
- [36] E. S. C. Ching, P.-Y. Lai, and C. Y. Leung, *Phys. Rev. E* **88**, 042817 (2013).
- [37] M. Timme and J. Casadiego, *J. Phys. A: Math. Theo.* **47**, 343001 (2014).
- [38] R.-Q. Su, Y.-C. Lai, and X. Wang, *Entropy* **16**, 3889 (2014).
- [39] R.-Q. Su, Y.-C. Lai, X. Wang, and Y.-H. Do, *Sci. Rep.* **4**, 3944 (2014).
- [40] Z.-S. Shen, W.-X. Wang, Y. Fan, Z. Di, and Y.-C. Lai, *Nat. Commun.* **5**, 4323 (2014).
- [41] E. S. C. Ching, P.-Y. Lai, and C. Y. Leung, *Phys. Rev. E* **91**, 030801 (2015).
- [42] R.-Q. Su, W.-W. Wang, X. Wang, and Y.-C. Lai, *R. Soc. Open Sci.* **3**, 150577 (2016).
- [43] J.-W. Li, Z.-S. Shen, W.-X. Wang, C. Grebogi, and Y.-C. Lai, *Phys. Rev. E* **95**, 032303 (2017).
- [44] C. Ma, H.-F. Zhang, and Y.-C. Lai, *Phys. Rev. E* **96**, 022320 (2017).
- [45] O. Feinerman, A. Rotem, and E. Moses, *Nat. Phys.* **4**, 967 (2008).
- [46] J. Soriano, M. R. Martínez, T. Tlustý, and E. Moses, *Proc. Nat. Acad. Sci. (USA)* **105**, 13758 (2008).
- [47] K. J. Friston, *NeuroImage* **16**, 513 (2002).
- [48] S. Pajevic and D. Plenz, *PLoS Comp. Biol.* **5**, e1000271 (2009).
- [49] S. Foucart and H. Rauhut, *A Mathematical Introduction to Compressive Sensing* (Birkhäuser, New York, 2013).
- [50] X. Han, Z.-S. Shen, W.-X. Wang, and Z.-R. Di, *Phys. Rev. Lett.* **114**, 028701 (2015).
- [51] W.-X. Wang, Y.-C. Lai, and C. Grebogi, *Phys. Rep.* **644**, 1 (2016).
- [52] R. Pastor-Satorras, C. Castellano, P. Van Mieghem, and A. Vespignani, *Rev. Mod. Phys.* **87**, 925 (2015).
- [53] A. Kumar, S. Rotter, and A. Aertsen, *Nat. Rev. Neurosci.* **11**, 615 (2010).
- [54] G. Szabó and G. Fath, *Phys. Rep.* **446**, 97 (2007).
- [55] W.-B. Du, X.-B. Cao, M.-B. Hu, and W.-X. Wang, *EPL (Europhys. Lett.)* **87**, 60004 (2009).
- [56] Y. Wang, G. Xiao, and J. Liu, *New J. Phys.* **14**, 013015 (2012).
- [57] Y.-Z. Chen and Y.-C. Lai, *arXiv* **1611:01849** (2016).
- [58] B. Ball, B. Karrer, and M. E. Newman, *Phys. Rev. E* **84**, 036103 (2011).
- [59] C. De Bacco, E. A. Power, D. B. Larremore, and C. Moore, *Phys. Rev. E* **95**, 042317 (2017).
- [60] X. Zhao, B. Yang, X. Liu, and H. Chen, *Phys. Rev. E* **95**, 042313 (2017).
- [61] X. Zhang, T. Martin, and M. E. Newman, *Phys. Rev. E* **91**, 032803 (2015).
- [62] M. E. J. Newman, *Phys. Rev. E* **94**, 052315 (2016).
- [63] M. E. J. Newman and G. Reinert, *Phys. Rev. Lett.* **117**, 078301 (2016).
- [64] B. Karrer and M. E. J. Newman, *Phys. Rev. E* **83**, 016107 (2011).
- [65] A. P. Dempster, N. M. Laird, and D. B. Rubin, *J. Royal Stat. Soc. Ser. B (Meth.)* **39**, 1 (1977).
- [66] T. Needham, *Ame. Math. Monthly* **100**, 768 (1993).
- [67] J. Davis and M. Goadrich, in *Proceedings of the 23rd international conference on Machine learning (ACM, 2006)* pp. 233–240.
- [68] P. Erdos and A. Rényi, *Publ. Math. Inst. Hung. Acad. Sci* **5**, 17 (1960).
- [69] A.-L. Barabási and R. Albert, *Science* **286**, 509 (1999).
- [70] D. J. Watts and S. H. Strogatz, *Nature* **393**, 440 (1998).
- [71] D. M. Powers, *J. Mach. Learning Tech.* **2**, 37 (2011).
- [72] V. Sood and S. Redner, *Phys. Rev. Lett.* **94**, 178701 (2005).
- [73] A. Kirman, *Quar. J. Econ.* **108**, 137 (1993).
- [74] P. L. Krapivsky, S. Redner, and E. Ben-Naim, *A Kinetic View of Statistical Physics* (Cambridge University Press, 2010).
- [75] D. M. Abrams and S. H. Strogatz, *Nature* **424**, 900 (2003).
- [76] M. Granovetter, *Ame. J. Sociol.* **83**, 1420 (1978).
- [77] M. J. de Oliveira, *J. Stat. Phys.* **66**, 273 (1992).